

VI. MICROWAVE SPECTROSCOPY*

Prof. M. W. P. Strandberg
Prof. R. L. Kyhl
Dr. D. H. Douglass, Jr.
J. M. Andrews
W. J. C. Grant

R. Huibonhoa
J. G. Ingersoll
P. F. Kellen
J. D. Kierstead

J. W. Mayo
W. J. Schwabe
J. R. Shane
N. Tepley
S. H. Wemple

RESEARCH OBJECTIVES

A large part of the activity of the Microwave Spectroscopy group, both experimental and theoretical, involves electron paramagnetic resonance. Much of this work involves the study of paramagnetic centers in crystalline solids at microwave frequencies. In general, we are trying to achieve an understanding of, and the development of a description for, the physical behavior of paramagnetic materials from a quantum-mechanical standpoint. Interest centers here, as well as in many other laboratories, on interaction mechanisms: spin-spin, spin-lattice and associated relaxation, line shape, and saturation phenomena. Similar studies are being made on liquid paramagnetic materials.

Electron paramagnetic resonance in gases is being used as a sensitive analytic tool for studying atomic recombination and diffusion rates of discharge products.

Problems associated with the design and operation of quantum-mechanical amplifiers are being investigated on solid-state masers and, to a lesser degree, on lasers and beam masers.

This laboratory is now also engaged in the investigation of the properties of metals and other materials at low temperatures. Particular emphasis is being placed on thin metallic films. Studies now in progress include a search among the transition and rare-earth-metal thin films for superconductors, an investigation of electron tunneling on single crystals of various superconductors, and a quantitative investigation of how the transition temperature of superfluid helium changes with the size of the specimen.

R. L. Kyhl, D. H. Douglass, Jr.

A. ELECTRON PARAMAGNETIC RESONANCE IN FERROELECTRIC POTASSIUM TANTALATE

A study is under way to examine the suitability of single-crystal potassium tantalate (KTaO_3) as a host lattice for certain iron group paramagnetic ions. We chose KTaO_3 as an interesting host possibility because it exhibits a phase transition from a simple cubic perovskite structure to a distorted ferroelectric phase near the temperature of liquid helium (4.2°K). This very low Curie transition enables us to conduct the electron paramagnetic resonance experiment at a temperature at which the spectrometer sensitivity is high, and, at the same time, enables us to hold the temperature of the crystal just above its Curie transition, at which point electrostrictive strain coefficients may be exceedingly large. Briefly, then, this study is concerned with electrostrictive tuning of paramagnetic energy levels in doped KTaO_3 .

*This work was supported in part by the U.S. Army Signal Corps under Contract DA36-039-sc-87376; and in part by Purchase Order DDL B-00306 with Lincoln Laboratory, a center for research operated by Massachusetts Institute of Technology with the joint support of the U.S. Army, Navy, and Air Force under Air Force Contract AF19(604)-7400.

(VI. MICROWAVE SPECTROSCOPY)

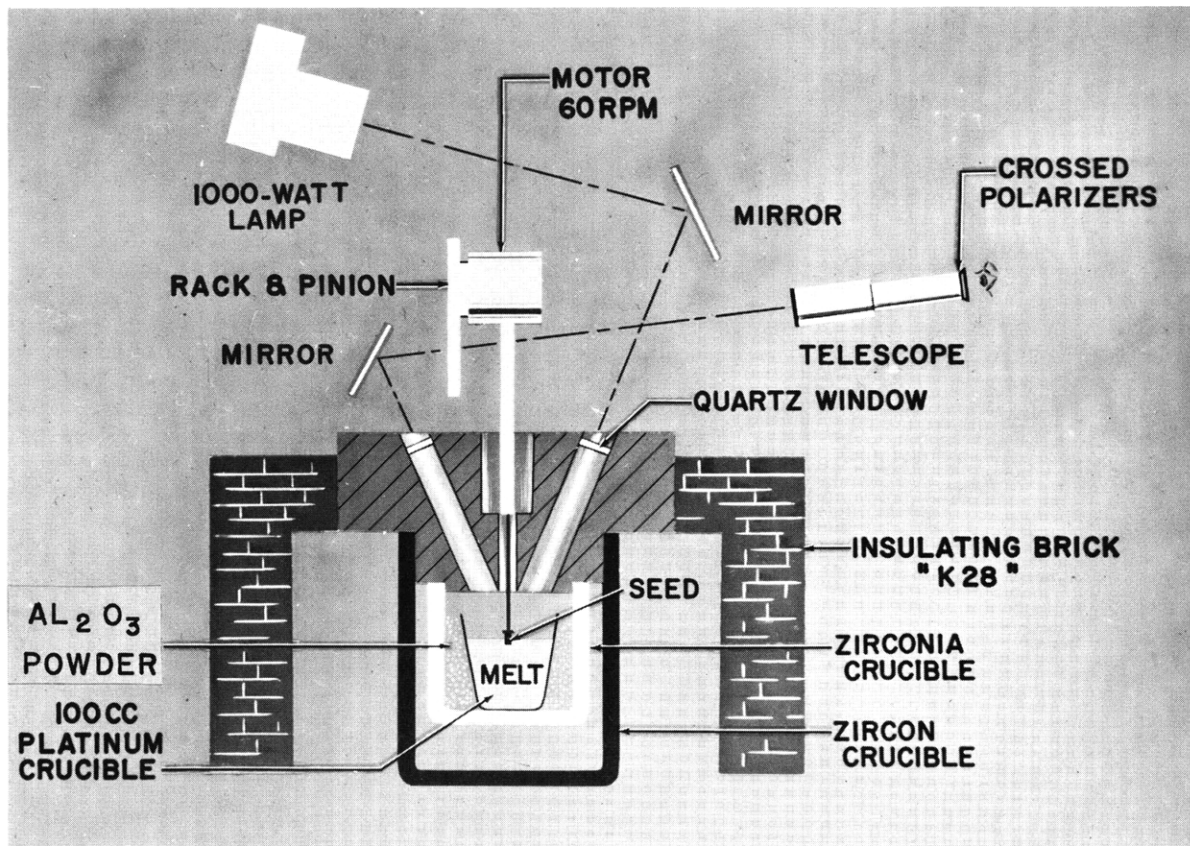


Fig. VI-1. The crystal-growing furnace.

Thus far the major effort has been devoted to growth of good single crystals of potassium tantalate. A flux method described by J. P. Remeika,¹ who used potassium fluoride, was discarded because only dark, small, highly conductive crystals were produced. A second method has proved quite satisfactory and is essentially the technique used by C. E. Miller² to grow single crystals of potassium niobate. The crystal-growing apparatus is shown schematically in Fig. VI-1. The melt is contained in a 100-cc platinum crucible and consists simply of Ta_2O_5 and a stoichiometric excess of K_2CO_3 (or K_2O since CO_2 is driven off during heating). Therefore, no extraneous or contaminating ions are introduced into the melt as they are in the flux method. An approximate partial phase diagram³ for the Ta_2O_5 - K_2O system is shown in Fig. VI-2. Selection of approximately 64 mole per cent K_2O results in precipitation of the desired $KTaO_3$ while cooling the melt from approximately $1250^\circ C$ to $1100^\circ C$. Because a seed method is used, as shown in Fig. VI-1, the liquidus temperature must be accurately determined. To accomplish this, light from a 1000-watt lamp is projected onto the melt surface and the reflected light observed through a telescope and crossed polarizers. A very tiny sliver of $KTaO_3$ is then dropped onto the surface and observed through the

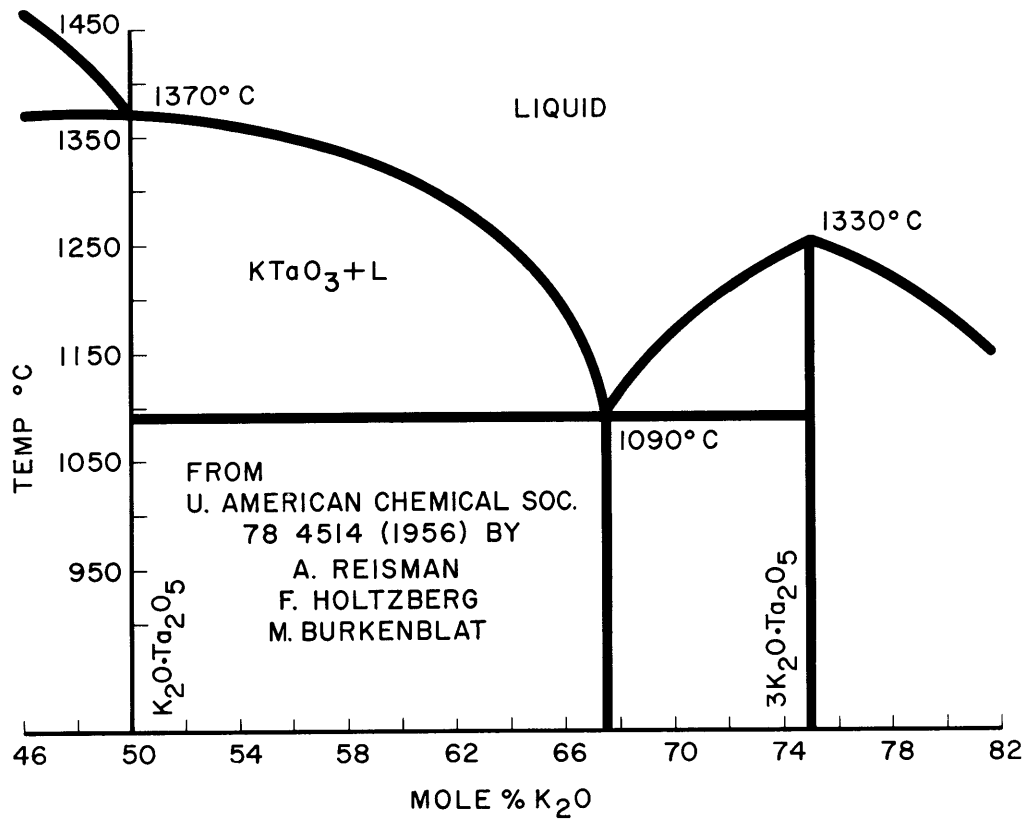


Fig. VI-2. Partial phase diagram for the Ta_2O_5 - K_2O system.

telescope. The "floating" sliver is clearly visible, and in this way the melt temperature can be adjusted to two or three degrees above the liquidus temperature at which point the test seeds dissolve in approximately 30 seconds to 1 minute. The growth seed, usually 3 or 4 mm square, is tied to the end of a 0.125-inch platinum rod with platinum wire. This seed is lowered so as to touch the melt and then retracted slightly but not far enough to break the meniscus. Crystal growth takes place while the seed rotates at 60 rpm. The direction of rotation is reversed every 30 seconds. Cooling the melt to approximately 1100°C at the rate of approximately 4°C per hour results in KTaO_3 crystals that weigh roughly 20 grams. As growth progresses the rotating crystal is lifted a total of 5-10 mm during the 24- to 30-hour growth period. Pulling is in a series of manual steps every 4-6 hours and is not continuous. At some temperature above 1090°C, at which the eutectic begins to form, the newly grown crystal is lifted approximately 1 cm above the melt surface and the entire crystal is cooled to room temperature over a period of 3-4 days.

Occasionally the foregoing method failed to work because an immiscible foreign liquid layer appeared to float on the melt surface, thereby preventing accurate determination

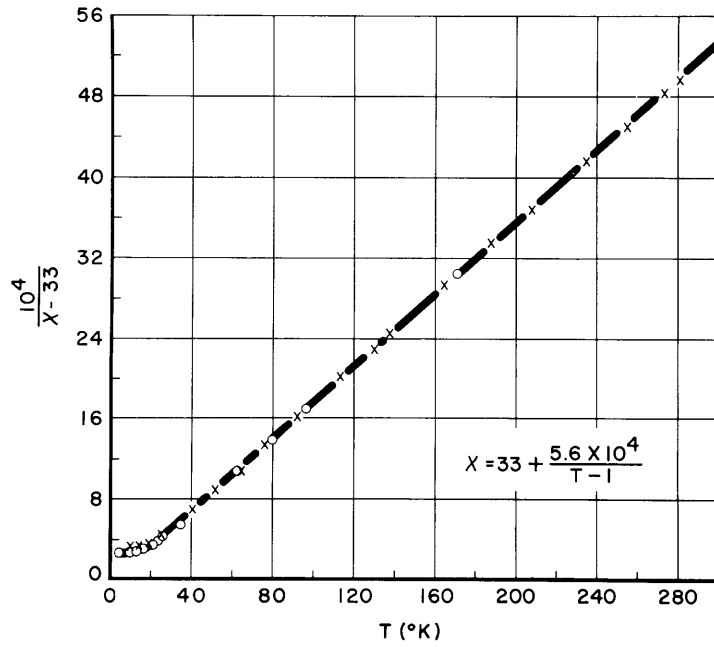


Fig. VI-3. Curie-Weiss curve for potassium tantalate.

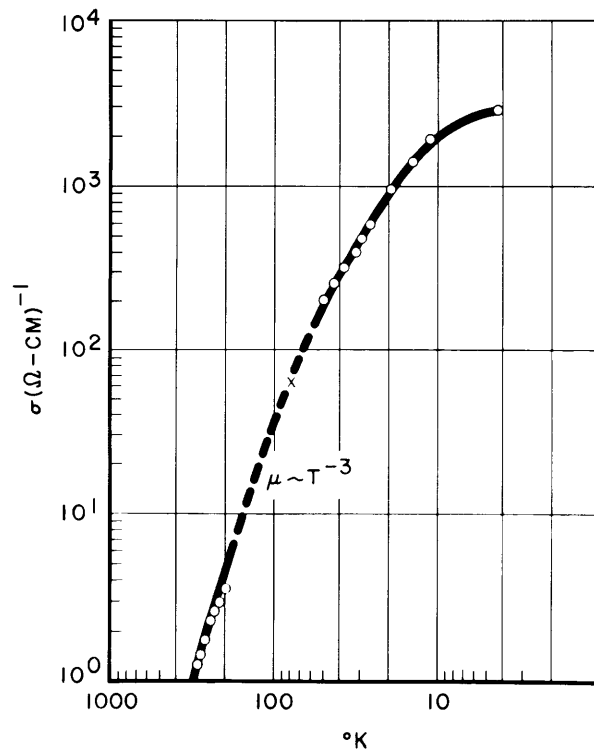


Fig. VI-4. The dc electrical conductivity vs temperature for KTaO_3 .

(VI. MICROWAVE SPECTROSCOPY)

of the liquidus temperature. This difficulty has been traced to calcium impurities in the Ta_2O_5 . For this reason purchase of Ta_2O_5 has had to be on a selective basis, with only those batches having less than 10 parts per million calcium acceptable.

Several $KTaO_3$ crystals have been grown. Undoped samples that were grown from Kawecki Chemical Company's optical grade Ta_2O_5 are transparent and colorless with an absorption edge at 0.350 microns and transparency to approximately 7 microns in the near infrared. The average index of refraction in the visible range is 2.6, and the electrical resistivity at room temperature is approximately 10^{12} ohm-cm. Figure VI-3 shows a Curie-Weiss plot of $10^4/(\chi - 33)$ vs temperature for this material. At room temperature the low-frequency dielectric constant is approximately 220. From Fig. VI-3 the extrapolated Curie temperature is seen to be $1^\circ K$. The $KTaO_3$ crystals grown from melts that are believed to be silicon-contaminated are found to have quite different properties. These crystals are very pale blue and are excellent electrical conductors, as shown in Fig. VI-4. Hall-effect measurement at room temperature indicates electron conduction with a mobility of $28 \text{ cm}^2/\text{volt-sec}$. A cyclotron-resonance study of this material might be exceedingly interesting.

Addition of 0.2 mole per cent Fe_2O_3 to the low-silicon melt results in pale yellow crystals that exhibit a rather complicated electron paramagnetic resonance spectrum consisting of 10 lines at room temperature in the magnetic field region below 8000 oersted. The spectrum exhibits cubic symmetry as expected. Further work on paramagnetically doped samples is now in progress.

S. H. Wemple

References

1. J. P. Remeika (private communication, July 1960).
2. C. E. Miller, J. Appl. Phys. 29, 233 (1958).

B. LINE SHAPES OF PARAMAGNETIC CHROMIUM RESONANCE IN RUBY

The line shapes of the main resonances in ruby present a source for several problems concerning the interactions of the paramagnetic chromium spins. Magnetic dipole interactions between chromium ions, and between chromium and neighboring aluminum nuclei, as well as exchange coupling between near neighbors, exert significant effects on the line shape. A theoretical understanding of the line shape is in turn a prerequisite for calculations that require the total area of the line, or the behavior of the line in the far wings, neither of which is directly observable. Examples are concentration measurements by electron paramagnetic resonance methods and quantitative application of cross-relaxation theory.

(VI. MICROWAVE SPECTROSCOPY)

Existing theories of line shapes depend on moment calculations.¹ Moments higher than the second are, unfortunately, exceedingly cumbersome to calculate, and the second moment alone can not be related to an experimental halfwidth without previous knowledge of the line shape. For ruby, the calculated second moment appears to mismatch that of the experimental halfwidths,² and does not seem to satisfactorily explain the concentration dependence of the halfwidth.³

With the calculations presented here we obtain the complete line shape that is derivable from dipolar interaction. The calculation is discussed, somewhat arbitrarily, in four steps:

1. We solve precisely the problem of two interacting dipoles. Neglect of N body interactions introduces an error of order $(n)^{N-2}$, where n is the spin concentration. Here, $N = 3$, $n < 0.01$, so the neglect of higher-order interactions gives an error of less than 1 per cent.

2. We formulate a statistical scheme for summing all of the pair interactions throughout the crystal. Random distribution of spins is assumed over the long range, but we leave open the possibility of short-range clustering.

3. We evaluate the integrals appearing in our formulation – a tedious, and not quite straightforward, process. In this way, we arrive at the logarithm of the Fourier transform of the resonance line.

4. We use machine computations to complete our calculations.

Step 1. The two-body Hamiltonian is

$$\mathcal{H} = g\beta\hat{H} \cdot (\hat{S}_1 + \hat{S}_2) - D(S_{z_1}^2 + S_{z_2}^2) + J\hat{S}_1 \cdot \hat{S}_2 + \frac{g^2\beta^2}{r^3} \left[\hat{S}_1 \cdot \hat{S}_2 - \frac{3(\hat{r} \cdot \hat{S}_1)(\hat{r} \cdot \hat{S}_2)}{r^2} \right]. \quad (1)$$

The terms, reading from left to right, represent Zeeman energy, crystal field splitting, exchange interaction, dipolar interaction. The physical situation includes cases in which J is large and in which J is small. Accordingly we have derived the 16×16 Hamiltonian matrix in the representations specified by

$$\psi_{JM} = \sum_{m_1} C(j_1, j_2, J; m_1, M-m_1, M) \psi_{j_1, m_1} \psi_{j_2, M-m_1} \quad (2)$$

and

$$\psi_{m_1 m_2} = \frac{1}{\sqrt{2}} \left(\psi_{m_1}^{(1)} \psi_{m_2}^{(2)} \pm \psi_{m_2}^{(1)} \psi_{m_1}^{(2)} \right). \quad (3)$$

The coupled scheme yields four submatrices corresponding to $\hat{S}_1 \cdot \hat{S}_2 = 6, 3, 1, 0$ with only high-order transitions occurring between the different blocks. The transitions within the 3-block have $\Delta E \approx g\beta H$ and can be expected to affect the corresponding main

(VI. MICROWAVE SPECTROSCOPY)

ruby line. Among the transitions in the 6-block, there are two with $\Delta E \approx g\beta H \pm 2D$, respectively, so that here, too, we can expect some effect on the corresponding main lines. The uncoupled case has 18 transitions, 6 of which are clustered around each of the one-ion transitions. The six differ from each other in transition probability and in the perturbation induced by dipolar energy and exchange. In Table VI-1 these transitions are tabulated according to the following notation: transition probability = g ; energy perturbation = $s \cdot \frac{g^2 \beta^2}{r^3} (3 \cos^2 \theta - 1) + t \cdot J$.

Step 2. The statistical summing over pairs adopts the point of view used in Margenau's work on line shapes of gases.⁴ We consider some atom for which, in the

Table VI-1. Energy perturbations and transition probabilities for uncoupled pair transitions.

$\Delta E_o = g\beta H - 2D$			$\Delta E_o = g\beta H$			$\Delta G_o = g\beta H + 2D$		
g	s	t	g	s	t	g	s	t
3/2	-9/4	0	1	-3/4	3	3/2	9/4	0
3/4	3/2	-3/2	1	3/4	-3	3/4	-3/2	3/2
3/2	1/4	2	2	-3/2	-3/2	3/2	-1/4	-2
3/4	-1/2	-5/2	2	3/2	3/2	3/4	1/2	5/2
3/4	3/2	-3/2	1	-9/4	0	3/4	-3/2	3/2
3/4	3/2	3/2	1	9/4	0	3/4	-3/2	-3/2

absence of perturbations, $\Delta E = \hbar\omega_o$. For notational convenience, we work with a shifted spectrum so that $\omega_o \equiv 0$, and the total perturbation caused by all other atoms is ω . From the last term in (1) it is clear that ω is a function of the position coordinates and quantum states of all of the other atoms, relative to the one we are considering:

$$\omega = \omega(\vec{r}_1, \vec{r}_2, \dots, \vec{r}_N, q_1, q_2, \dots, q_N). \quad (4)$$

Each possible configuration of perturbers in this $4N$ -dimensional space gives some value of ω . The intensity for some particular value of ω is given by

$$I(\omega) = \frac{1}{V^N} \int d\tau \dots d\tau_N dq_1 \dots dq_N \delta[\omega - \omega(\vec{r}_1, \dots, \vec{r}_N, q_1, \dots, q_N)] \quad (5)$$

where V is a normalization volume $\int d\tau dq$, and δ is a delta function. Replacing δ by

(VI. MICROWAVE SPECTROSCOPY)

its Fourier transform, we have

$$I(\omega) = \frac{1}{V^N} \int d\tau_1 \dots d\tau_N dq \dots dq_N \frac{1}{2\pi} \int_{-\infty}^{\infty} e^{-i\rho[\omega - \omega(\vec{r}_1 \dots \vec{r}_N, q_1 \dots q_N)]} d\rho. \quad (6)$$

Correlative to our approximation of neglecting N body interactions, $N \geq 3$, we have additivity of the two-body perturbations:

$$\omega(\vec{r}_1 \dots \vec{r}_N, q_1 \dots q_N) = \sum \omega_i(r_i, q_i). \quad (7)$$

This makes the integrals in (6) separable, and we have

$$I(\omega) = \frac{1}{2\pi} \int_{-\infty}^{\infty} e^{-i\rho\omega} \left[\frac{1}{V} \int d\tau dq e^{i\rho\omega(\vec{r}, q)} \right]^N d\rho. \quad (8)$$

For the sake of clarity, we consider for a moment a simpler problem, in which there is no multiplicity of quantum states and in which the integral over $d\tau$ can be taken at face value; that is, the distribution of perturbers is continuous and not confined to discrete lattice sites. The bracketed expression in (8), which assumes the form $\frac{\infty}{N}$ as $N \rightarrow \infty$, can then be handled as follows:

$$\frac{1}{V} \int d\tau e^{i\rho\omega(\vec{r})} = \frac{1}{V} \left[\int d\tau - \int d\tau (1 - e^{i\rho\omega(\vec{r})}) \right] = 1 - \frac{V'}{V} = 1 - \frac{n'V'}{N} \quad (9)$$

where

$$V' = \int d\tau (1 - e^{i\rho\omega(\vec{r})}) \quad (10)$$

and n' is the number of perturbers per unit volume. We now may write

$$\lim_{N \rightarrow \infty} \left[\frac{1}{V} \int d\tau e^{i\rho\omega(r)} \right]^N = \lim_{N \rightarrow \infty} \left(1 - \frac{n'V'}{N} \right)^N = e^{-n'V'}. \quad (11)$$

Returning to the complications peculiar to our problem, we work with the following model:

(a) We consider a lattice as far as a radius r_0 . Beyond r_0 , the angular density of lattice points is sufficiently great so that a continuous distribution may be used with negligible error.

(b) We use the close-coupled scheme for $r < r_1$, and the uncoupled scheme for $r > r_1$, where $r_1 < r_0$.

(c) We consider exchange effects to be negligible for $r > r_0$.

(VI. MICROWAVE SPECTROSCOPY)

One can show rigorously that steps (9)-(11) go through exactly as before, but with

$$\begin{aligned}
 V' = & \frac{1}{\sum_j g_j} \left[\sum_k g_k \sum_{r_i < r_1} (1 - e^{i\rho\omega(\hat{r}_i, \mathbf{s}_k)}) \right. \\
 & + \sum_j g_j \sum_{r_1 < r_i < r_0} (1 - e^{i\rho\omega(\hat{r}_i, \hat{\mathbf{s}}_j)}) \\
 & \left. + \frac{1}{v} \sum_j g_j \int d\Omega \int_{r_0}^{\infty} dr r^2 (1 - e^{i\rho\omega(\hat{r}, \mathbf{s}_j)}) \right] \quad (12)
 \end{aligned}$$

where g_k and \mathbf{s}_k refer to the relevant transition probabilities and quantum states in the coupled scheme, g_j and \mathbf{s}_j refer to the corresponding quantities in the uncoupled scheme, v is the volume per lattice site, and n is the molar concentration of perturbing spins.

Step 3. We must now evaluate

$$\int_{-1}^1 d \cos \theta \int_{r_0}^{\infty} dr r^2 \left[1 - \exp\left(\frac{isa}{r^3}\right) \right] \equiv V_j \quad (13)$$

where $a = \rho g^2 \beta^2 (3 \cos^2 \theta - 1)$. The substitution $x = \frac{1}{r^3}$ in (13) and a partial integration gives

$$\frac{1}{3} \int_{-1}^1 d \cos \theta \left[\frac{e^{isax_0}}{x_0} - \frac{1}{x_0} - isa - isa \int_0^{x_0} \frac{e^{isax}}{x} dx \right] \quad (14)$$

The first term in (14), after some transformations, yields

$$\frac{e^{-ic} e^{i(\pi/4)sgnc}}{x_0 \sqrt{3K}} \gamma\left(\frac{1}{2}, -3ic\right)$$

where $c = sg^2 \beta^2 \rho x_0$, $k = |c|$, and $\gamma(a, x)$ is the incomplete gamma function.⁵ The second and third terms trivially yield $\frac{-2}{x_0}$ and 0. The x integral in the fourth term diverges at $x = 0$. If we replace 0 by t , we obtain for this term

$$\int_{-1}^1 d \cos \theta \{ sa \text{Si}(sax_0) - isa \text{Ci}(sax_0) + isa \log |sax_0| + isa (\gamma - \log x_0) + isa \log t \} \quad (15)$$

The functions $\text{Si}(x)$ and $\text{Ci}(x)$ are those defined by Jahnke and Emde.⁶

We observe that the logarithmic divergence is independent of θ . If the integration over θ were continuous, instead of being an approximation to a lattice sum, then

(VI. MICROWAVE SPECTROSCOPY)

$\int_{-1}^1 d\cos\theta (3\cos^2\theta - 1) \log t$ would still go to zero. Actually, $t \rightarrow 0$ corresponds to $r^3 \rightarrow \infty$. Analysis shows that under these circumstances the sum over θ "becomes continuous" faster than $\log t$ becomes infinite; that is, the summation over angles does in fact kill the radial divergence. Stated in physical terms, an energy perturbation that falls off as $1/r^3$, or slower, gives a diverging effect as r increases. We are spared this catastrophe, however, because the angular dependence of the perturbation produces sufficient cancellation.

The functions $\text{Si}(y)$ and $[\log y - \text{Ci}(y)]$ are entire functions, so that there is no intrinsic ambiguity in (15). To be able to continue, however, we must handle $\log y$ and $\text{Ci}(y)$ separately, and each has a branch point at the origin. Care is needed to treat both singularities in an identical manner.

After a few more changes of variable, interspersed with partial integrations, (15) is brought into the form

$$\frac{2i}{3x_0\sqrt{3c}} \left[e^{-ic} \int_0^{3c} \left(1 - \frac{2c}{W-c}\right) W^{1/2} e^{iW} dW - \int_0^{3c} \left(1 - \frac{2c}{W-c}\right) W^{1/2} dW \right]. \quad (16)$$

Each integral has a pole at $W = c$ and a branch point at $W = 0$. To guarantee equal treatment, we evaluate the integral

$$\int_0^{3c} \left(1 - \frac{2c}{W-c}\right) W^{1/2} e^{ixW} dW \quad (17)$$

and then specialize to $x = 1$ and $x = 0$. With $u = xW$ and $c' = xc$, (17) becomes

$$x^{-3/2} \int_0^{3c'} \left(1 - \frac{2c'}{u-c'}\right) u^{1/2} e^{iu} du. \quad (18)$$

After a little maneuvering, the first term in (18) gives

$$\left(\frac{i}{x}\right)^{3/2} \gamma(3/2, -3ic'). \quad (19)$$

For $x = 1$, we use the well-known recursion relation for γ functions to obtain

$$\frac{1}{2} i^{3/2} \gamma\left(\frac{1}{2}, -3ic\right) - i(3c)^{1/2} e^{3ic}. \quad (20)$$

For $x = 0$, the expansion

$$\gamma(a, x) = \sum_{n=0}^{\infty} \frac{(-)^n x^{a+n}}{n!(a+n)} \quad (21)$$

reduces (19) to $\frac{2}{3} (3c)^{3/2}$.

The second term in (18) is handled by means of the following scheme:

$$\int_0^{3c'} \frac{u^{1/2}}{u-c'} e^{iu} du = \int_0^\infty \frac{u^{1/2}}{u-c'} e^{iu} du - \int_{3c'}^\infty \frac{u^{1/2}}{u-c'} e^{iu} du. \quad (22)$$

The \int_0^∞ is evaluated as a contour integral in the complex u plane. For $c' > 0$, we choose the path shown in Fig. VI-5. Thus we obtain

$$\int_0^\infty = \pi i (k')^{1/2} e^{ik'} + i^{1/2} \int_0^\infty \frac{y^{1/2} e^{-y} dy}{y + ik'} \quad (23)$$

$$\int_0^\infty = \pi i (k')^{1/2} e^{ik'} + (\pi i)^{1/2} - i\pi^{1/2} e^{ik'} (k')^{1/2} \Gamma\left(\frac{1}{2}, ik'\right) \quad (24)$$

As before, $k' = |c'|$.

The $\int_{3c'}^\infty$ is evaluated by expanding $\frac{1}{u-c'}$ in descending powers of u and substituting $u = 3k'(t+1)$. Each member of the series then turns out to be an integral representation of the confluent hypergeometric function, $\psi\left(1, \frac{3}{2}-n; -i3k'\right)$, and, using equations⁷ given by Bateman, we obtain

$$\int_{3c'}^\infty \frac{u^{1/2}}{u-c'} e^{iu} du = \sum_{n=0}^\infty (k')^n (-i)^{n-1/2} \Gamma\left(-n + \frac{1}{2}, -3ik'\right). \quad (25)$$

For $c' < 0$, it can be seen by inspection of (16) or (22), or even (13), that the result will be i times the complex conjugate of the result for $c' > 0$.

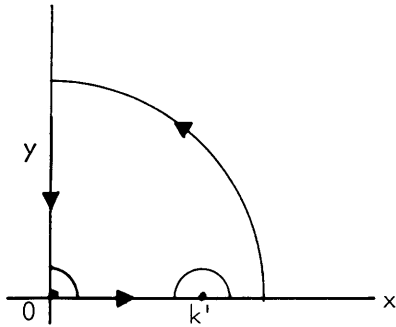


Fig. VI-5. Integration path for $c' > 0$ in the complex u plane.

Specializing to $x = 1$ is trivial, and merely involves replacing k' by k and c' by c . Specializing to $x = 0$ again involves the series expansions for incomplete gamma functions. The second integral of (16) then becomes

(VI. MICROWAVE SPECTROSCOPY)

$$\int_0^{3c} \frac{W^{1/2}}{W-C} dW = c^{1/2} \log \left(\frac{\sqrt{3}+1}{\sqrt{3}-1} \right) - 2\sqrt{3}c. \quad (26)$$

A more direct approach to this integral will give an error of π times the residue at c . Tabulated integrals give a Cauchy principal value, but we have clearly not taken the corresponding path (—) around c , in the partner integral.

Finally, we collect the integrated terms to obtain

$$\begin{aligned} V_j = \frac{4}{3\sqrt{3}x_0} & \left\{ \pi k + \left(\sqrt{3} + \log \frac{\sqrt{3}-1}{\sqrt{3}+1} \right) ic - \sqrt{\pi} k \Gamma \left(\frac{1}{2}, ic \right) \right. \\ & + (-i\pi c)^{1/2} e^{-ic} + \frac{1}{2} e^{-ic} (-ic)^{-1/2} \gamma \left(\frac{1}{2}, -3ic \right) \\ & \left. - e^{-ic} \sum_{n=0}^{\infty} (-ic)^{n+1/2} \Gamma \left(-n + \frac{1}{2}, -3ic \right) + \frac{\sqrt{3}}{2} (e^{2ic} - 3) \right\} \quad (27) \end{aligned}$$

To cast this result in a form suitable for computation, we expand it into an ascending series and an asymptotic series:

Ascending series:

$$\text{Re } V_j = \frac{4}{3x_0} \left[\frac{1}{2} \cos 2c - \frac{3}{2} + \cos c \sum_{\substack{m=0 \\ m \text{ even}}}^{\infty} a_m c^m + \sin c \sum_{\substack{m=1 \\ m \text{ odd}}}^{\infty} a_m c^m \right] \quad (28)$$

$$\text{Im } V_j = \frac{4}{3x_0} \left[c + \frac{1}{2} \sin 2c + \cos c \sum_{\substack{m=1 \\ m \text{ odd}}}^{\infty} a_m c^m - \sin c \sum_{\substack{m=0 \\ m \text{ even}}}^{\infty} a_m c^m \right] \quad (29)$$

$$a_m = \frac{1}{m!} \left(3^m - m \sum_{p=0}^m \frac{3^p}{p + \frac{1}{2}} \right) \quad (30)$$

Asymptotic series:

$$\begin{aligned} \text{Re } V_j = \frac{4}{3x_0} & \left\{ \frac{\pi k}{\sqrt{3}} - \frac{3}{2} - \sqrt{\frac{\pi}{3}} k^{1/2} \left[\cos \left(k + \frac{\pi}{4} \right) \sum_{\substack{m=2 \\ m \text{ even}}}^{\infty} b_m k^{-m} + \sin \left(k + \frac{\pi}{4} \right) \sum_{\substack{m=3 \\ m \text{ odd}}}^{\infty} b_m k^{-m} \right] \right. \\ & \left. + \cos 2k \sum_{\substack{m=2 \\ m \text{ even}}}^{\infty} \beta_m (3k)^{-m} - \sin 2k \sum_{\substack{m=3 \\ m \text{ odd}}}^{\infty} \beta_m (3k)^{-m} \right\} \quad (31) \end{aligned}$$

$$\text{Im } V_j = \pm \frac{4}{3x_0} \left\{ -\sqrt{\frac{\pi}{3}} k^{1/2} \left[\cos \left(k + \frac{\pi}{4} \right) \sum_{\substack{m=3 \\ m \text{ odd}}}^{\infty} b_m k^{-m} - \sin \left(k + \frac{\pi}{4} \right) \sum_{\substack{m=2 \\ m \text{ even}}}^{\infty} b_m k^{-m} \right] \right. \\ \left. + \cos 2k \sum_{\substack{m=3 \\ m \text{ odd}}}^{\infty} \beta_m (3k)^{-m} + \sin 2k \sum_{\substack{m=2 \\ m \text{ even}}}^{\infty} \beta_m (3k)^{-m} \right\} \quad (32)$$

Here, the upper sign is for $c > 0$, the lower sign for $c < 0$,

$$b_m = \left(\frac{1}{2} \right)_m \quad (33)$$

$$\beta_m = \frac{1}{2} \left(\frac{1}{2} \right)_{m-1} - \sum_{p=0}^{\infty} 3^{-p-1} \left(p + \frac{1}{2} \right)_m. \quad (34)$$

In (33) and (34) the notation $(a)_n$ means $(a)_n = a(a+1)(a+2) \dots (a+n-1)$, with $(a)_0 = 1$.

The expression $\exp \left(-\frac{n}{v} \cdot \frac{2\pi}{3} \frac{\sum g_j V_j}{\sum g_j} \right)$ represents the contribution of atoms that are located at $r > r_0$ to the Fourier transform of the resonance line. If one looks at the leading terms in the ascending series and the asymptotic series given above, one finds that this transform has, at least qualitatively, the expected properties. Asymptotically

it behaves like an exponential of the form $\exp(-a|\rho|)$, with $a = (n/v)(8\pi^2/9\sqrt{3}) \frac{\sum |s_j g_j|}{\sum g_j}$.

This implies that the line is Lorentzian near the origin, with halfwidth equal to a . Near the origin, the transform looks like a Gaussian; this, in turn, implies a Gaussian behavior of the line in the far wings.

We notice that the real part of V_j is symmetric in ρ and c , while the imaginary part is antisymmetric. As a consequence, for cases in which $\sum g_j s_j = 0$, the imaginary part vanishes. If we had assumed this condition at the outset, the calculation would have been enormously simplified. Actually, this condition does hold in general as a consequence of spectroscopic stability, if the entire spectrum is considered. But for individual lines it does not necessarily hold. The effect on the line shape of $\sum g_j s_j \neq 0$ is the production of an asymmetry. Thus, nonsymmetric lines and nonvanishing odd moments are possible.

If desired, all of the moments of the line can be obtained at this point. If

$$I(\omega) = \int_{-\infty}^{\infty} e^{-i\omega\rho} F(i\rho) d\rho$$

then

(VI. MICROWAVE SPECTROSCOPY)

$$\langle \omega^m \rangle = (-)^m \left. \frac{\partial^m F(i\rho)}{\partial (i\rho)^m} \right|_{\rho=0} . \quad (35)$$

Here, $F = \exp[-nV'(i\rho)]$, and $F(0) = 1$. These relations give

$$F^{(m)}(0) = (-)^{m+1} nV'^{(m)}(0) + \text{higher terms in } n. \quad (36)$$

Now $V'^{(m)}(0)$ is simply the m^{th} coefficient of the Taylor series for V' . This series can be obtained by expanding the trigonometric functions in (28) and (29) in Taylor series and taking Cauchy products. The result is

$$\begin{aligned} \langle \omega^0 \rangle &= 1 \\ \langle \omega^1 \rangle &= 0 \\ \langle \omega^m \rangle_{m>1} &= (-)^{m+1} \left(\frac{n}{v} \cdot \frac{2\pi}{3} \cdot \frac{\sum g_j V_j^{(m)}(0)}{\sum g_j} \right) \end{aligned} \quad (37)$$

with

$$V_j^{(m)}(0) = 2^{m-1} + \frac{1}{m!} \sum_{k=0}^m \left(3^k - k \sum_{p=0}^k \frac{3^p}{p + \frac{1}{2}} \right) \binom{m}{k} (-)^{m-k} \quad (38)$$

where $\binom{m}{k}$ are binomial coefficients.

Finally, in regard to r_o and x_o , we have made a rather elaborate analysis of the error that is introduced as a result of integrating over continuous coordinate variables rather than summing over lattice sites, from some r_o outward. The choice of $r_o = 6.3 \text{ \AA}$, halfway between the 13th and 14th neighbor shells, is expected to introduce an error of approximately 1.0 per cent as a result of this approximation.

Step 4. We have computed the V_j 's, their weighted sums, and the transforms to which they lead. We have used the parameters g , s , and v that are appropriate to the transitions occurring in ruby with the crystal axis oriented parallel to the magnetic field. Figures VI-6 and VI-7 refer to the transition occurring at approximately 800 gauss at X-band, and

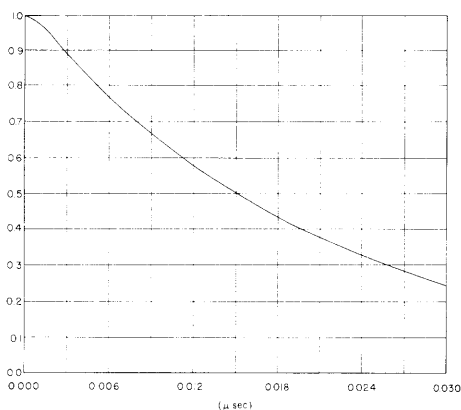


Fig. VI-6. Fourier transform (magnitude).

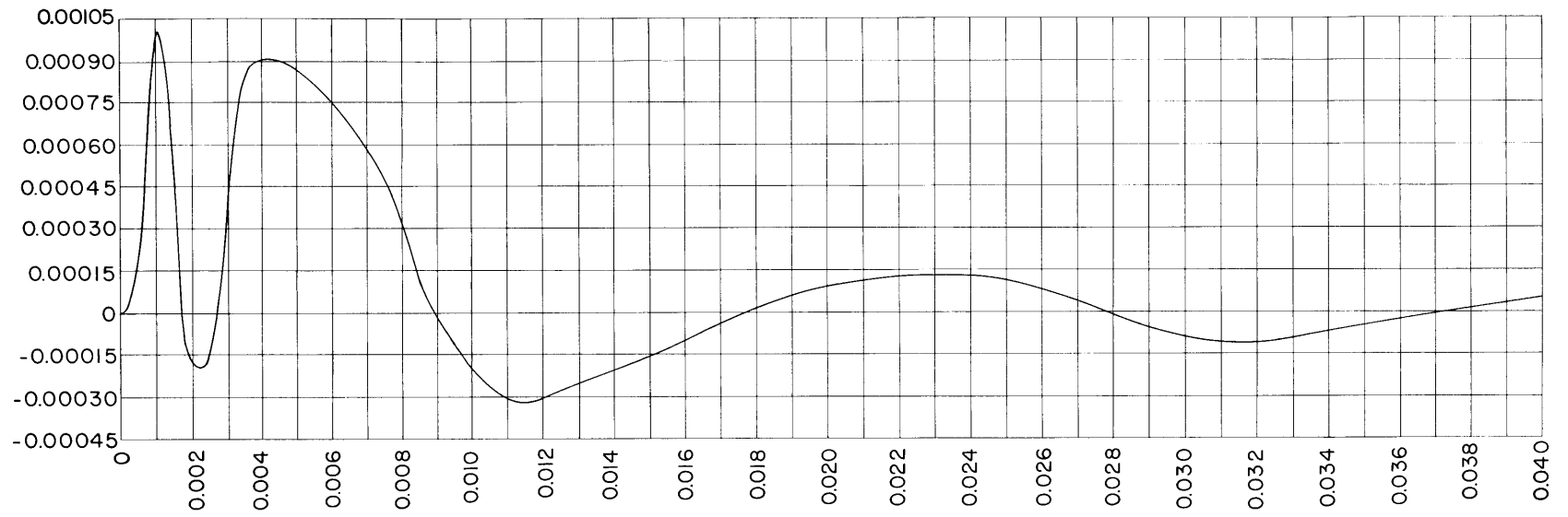


Fig. VI-7. Fourier transform (angle).

(VI. MICROWAVE SPECTROSCOPY)

are computed for a concentration of 0.1 per cent. They show, respectively, the magnitude and the angle of the complex transform. Although the nonzero angle implies an asymmetry in the line shape, it is apparent that the effect is too small for direct observation.

Actually, these curves are not exactly transforms of the resonance line, since the contribution from the lattice sites at $r < r_0$, as well as the dipole interaction with the surrounding Al nuclei, must still be included. We have worked out suitable computer routines for inverting the transform, and for including the last two effects by subsequent convolution. Final numerical results are not yet available.

W. J. C. Grant

References

1. J. H. Van Vleck, Phys. Rev. 74, 1168 (1948); and M. H. L. Pryce and K. W. H. Stevens, Proc. Phys. Soc. A63, 36 (1950).
2. A. A. Manenkov and V. B. Fedorov, J. Exptl. Theoret. Phys. 11, 751 (1960).
3. See C. Kittel and E. Abrahams, Phys. Rev. 90, 238 (1953) for one attempt to circumvent this difficulty.
4. H. Margenau, Phys. Rev. 48, 755 (1935); and H. Margenau and W. W. Watson, Revs. Modern Phys. 8, 22 (1936).
5. The functions $\gamma(a, x)$, their functional relations, integral representations, and expansions can be found in Higher Transcendental Functions (Bateman Manuscript Project), A. Erdelyi, F. Oberhettinger, W. Magnus, and F. G. Tricomi (eds.) (McGraw-Hill Book Company, Inc., New York, 1954), Vol. 2, Chap. 9.
6. E. Jahnke and F. Emde, Tables of Functions (Dover Publishers, New York, 1945), pp. 1-3.
7. A. Erdelyi, F. Oberhettinger, W. Magnus, and F. G. Tricomi, op. cit., cf. Eqs. 6.5.2 and 6.5.6, Vol. 1, Chap. 6.